

Probabilistic modelling of tephra dispersion

C. BONADONNA

Department of Geology, University of South Florida, Tampa, FL 33620-5201, USA

(e-mail: costanza@cas.usf.edu)

Depending on their magnitude and location, volcanic eruptions have the potential to become major social and economic disasters (e.g. Tambora, Indonesia, 1815; Vesuvius, Italy, AD 79; Soufrière Hills Volcano, Montserrat, 1995–present). One of the challenges for the volcanology community is to improve our understanding of volcanic processes so as to achieve successful assessments and mitigation of volcanic hazards, which are traditionally based on volcano monitoring and geological records. Geological records are crucial to our understanding of eruptive activity and history of a volcano, but often do not provide a comprehensive picture of the variation of volcanic processes and their effects on the surrounding area. The geological record is also typically biased towards the largest events, as deposits from smaller eruptions are often removed by erosion. Numerical modelling and probability analysis can be used to complement direct observations and to explore a much wider range of possible scenarios. As a result, numerical modelling and probabilistic analysis have become increasingly important in hazard assessment of volcanic hazards (e.g. Barberi *et al.* 1990; Heffter & Stunder 1993; Wadge *et al.* 1994, 1998; Hill *et al.* 1998; Iverson *et al.* 1998; Searcy *et al.* 1998; Canuti *et al.* 2002).

Reliable and comprehensive hazard assessments of volcanic processes are based on the critical combination of field data, numerical simulations and probability analysis. This paper offers a detailed review of common approaches for hazard assessments of tephra dispersion. First, the main characteristics of tephra dispersion and tephra hazards are recounted. A critical use of field data for a quantitative study of tephra deposits is also discussed. Second, numerical modelling typically used for hazard assessments of tephra accumulation is described. Finally, the most common probability analyses applied to hazard studies of tephra dispersion are presented.

The challenges of tephra dispersion and tephra hazards

Tephra is one of the main products of explosive eruptions and forms after material has been explosively

ejected from a vent to produce an eruptive column, which is a buoyant plume of tephra and gas rising high into the atmosphere. Tephra can also be dispersed from buoyant plumes overriding dome-collapse or column-collapse pyroclastic flows and generated for elutriation (i.e. co-pyroclastic-flow plumes). Elutriation is the process in which fine particles are separated from the heavier pyroclastic-flow material as a result of an upward-directed stream of gas. Tephra is then transported through the atmosphere and fractionated by the wind depending on particle size, density and shape. In this paper tephra is used in the original sense of Thorarinsson (1944) as a collective term for airborne volcanic ejecta irrespective of size, composition or shape.

The main components of tephra deposits are juvenile fragments (i.e. quenched pieces of fresh magma), lithic fragments (i.e. pieces of pre-existing rocks) and free crystals. Particle sizes can range from large blocks and bombs (>64 mm) to fine ash (<63 µm). Particle densities typically vary between *c.* 3000 kg m⁻³ (for dense crystals and lithic fragments) and *c.* 500 kg m⁻³ (for highly vesicular juveniles).

Production of tephra is not the most dangerous amongst volcanic phenomena, pyroclastic flows and lahars being the two most deadly volcanic processes (Baxter 1990). However, tephra can be transported in the atmosphere for long times and distances after the eruptive event, and represents one of the most widespread hazards, with several deadly consequences and the potential to significantly affect diverse economic sectors, such as agriculture, social services, tourism and industry. As an example, despite a massive and successful evacuation of people living within 30 km of the volcano, about 300 people died from the collapse of roofs under the weight of 5–50 cm of wet tephra in the 1991 eruption of Pinatubo (Philippines).

Volcanic ash suspended in the air soon after fallout and/or reworked even a few years after the eruptive event might contain a large proportion of respirable particles (<10 µm), which may induce a host of respiratory problems in unprotected susceptible people, including asthma, bronchitis, pneumonia and emphysema. Volcanic ash can also contain crystalline silica (i.e. quartz and its polymorphs), which may pose a potential hazard of silicosis and

lung cancer, and can incorporate toxic substances such as fluoride, which can kill a large number of grazing animals and endanger human drinking water supplies. In addition, windborne ash is also a serious threat to aircraft up to 3000 km from the eruptive vent, and accumulation of even a few millimetres of tephra can affect aircraft manoeuvring on runways, and cause airports to close for several days. Finally, massive production of tephra can also provide loose sediments for the generation of deadly lahars even several years after the eruptive event. As a result, the study of tephra dispersion represents an important aspect of hazard mitigation necessary in those populated areas that have developed close to active volcanoes and/or where there is significant aviation traffic.

Field investigations and their natural evolution

Field investigations are the first step towards a quantitative characterization of volcanic processes and they naturally evolve to complement associated studies of eruptive dynamics. Collection and analysis of field data were originally aimed at classifying the style of eruptive events and the type of pyroclastic deposits using thickness and grain-size data (Walker 1971, 1973). Distributions of deposit

thickness and grain-size characteristics were quantified by compiling isopach maps (Fig. 1a) and determining statistical parameters, respectively (e.g. median diameter, Md_{ϕ} , and deviation, σ_{ϕ} , of cumulative grain-size curves (Inman 1952; Walker 1971)). Grain-size analyses were typically carried out using standard sieving techniques, which are practical only for particles with diameter $>63 \mu\text{m}$.

Later, field data were also used to thoroughly quantify other important eruptive parameters, such as column height, wind speed, magnitude, intensity and grain-size distribution of the whole deposit, also defined as total grain-size distribution (e.g. Walker 1980; Carey & Sparks 1986; Pyle 1989). As a result, field data collection and processing were adjusted to account for specific features used in these models. For example, the distribution of specific particle sizes around the vent can be quantified by compiling isopleth maps (Fig. 1b) and used to determine the column height and wind speed at the time of the eruption (Carey & Sparks 1986).

For the benefit of hazard studies and a better understanding of volcanic processes, field investigations should evolve even further to account for specific requirements of numerical modelling and probability analysis of eruptive scenarios. Dispersion models are very sensitive to the choice of the total grain-size distribution. Therefore,

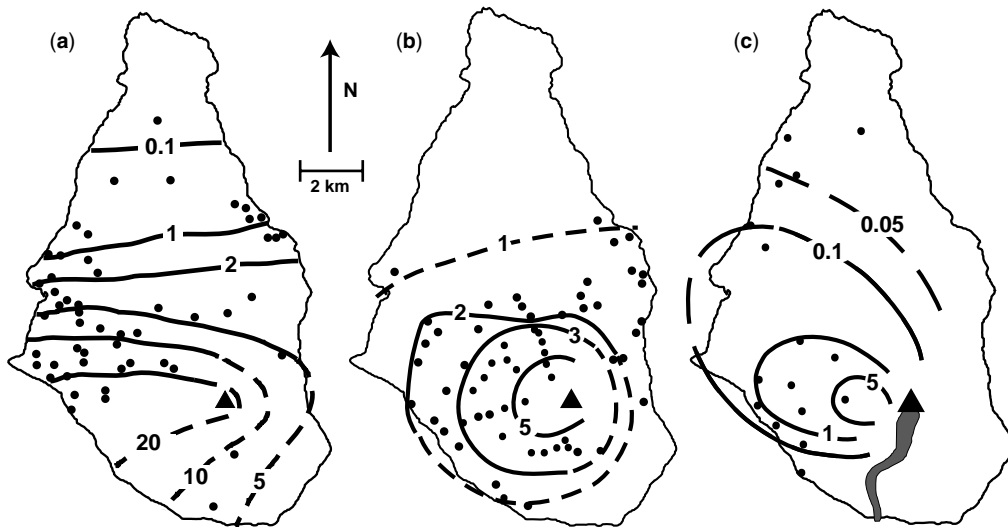


Fig. 1. Three styles of contour maps of tephra deposits for different periods of activity of the Soufrière Hills volcano, Montserrat. (a) Isopach map (cm) showing the cumulative thickness of all tephra accumulated between 4 August and 21 October 1997 (mainly from Vulcanian explosions). (b) Isopleth map showing mean diameter (cm) of the five largest lithic fragments for the 17 September 1996 sub-Plinian eruption. (c) Isomass map showing the distribution of co-pyroclastic flow tephra (in kg m^{-2}) generated from a small dome-collapse pyroclastic flow (31 March 1997). The grey area shows the associated pyroclastic-flow deposit. Dashed lines indicate contours constructed with limited field data (\bullet). Position of Soufrière Hills volcano is also shown (\blacktriangle). Data from Robertson *et al.* (1998) and Bonadonna *et al.* (2002b).

grain-size analysis should include fine ash (<63 μm) and individual grain-size distributions (i.e. distributions for each locality) should be integrated to provide the grain-size distribution for the whole deposit. Only a few complete total grain-size distributions are actually available in the literature (e.g. Sparks *et al.* 1981; Carey & Sigurdsson 1982; Bonadonna & Houghton 2005). In addition, the validity of Md_ϕ and σ_ϕ relies on the assumption that grain-size distributions are approximately log normal. More appropriate statistical parameters should be used to characterize grain-size distributions that are not log normal (e.g. polymodal distributions). Another important feature for the validation of numerical models is the identification of the contour line of zero mass or thickness. Therefore, some indications of localities where tephra accumulation is zero should be given. Finally, when multiple units are present in a stratigraphic record, it is crucial to distinguish the climactic phase from minor events, to define accurate eruptive scenarios. Thickness distribution for each phase is also easier to model and forecast than cumulative thickness. When feasible, distribution of mass per unit area (isomass maps, Fig. 1c) is preferred to isopach maps (Fig. 1a), to account for compaction of the deposit and for variation of deposit density with distance from the vent. Isomass maps are also easier to compare directly with outputs from numerical simulations, which are typically expressed as mass per unit area. As a result, in addition to the classic field parameters, field investigations should also provide detailed information on total grain-size distributions, lateral extent of deposit, stratigraphic record, deposit density, particle density and tephra accumulation per unit area.

Numerical investigations

Numerical investigations help reproduce those parts of the deposit that are not accessible or are partly or completely missing. They can also be used to simulate eruptive events that have not happened yet, but might eventually happen, providing a fundamental tool for hazard mitigation.

A number of studies of particle sedimentation from volcanic plumes have been based on the principles of particle advection and diffusion expressed by the following mass-conservation equation:

$$\begin{aligned} \frac{\partial C_j}{\partial t} + \frac{\partial(u_x C_j)}{\partial x} + \frac{\partial(u_y C_j)}{\partial y} + \frac{\partial(u_z C_j)}{\partial z} \\ = \frac{\partial^2(K_x C_j)}{\partial x^2} + \frac{\partial^2(K_y C_j)}{\partial y^2} + \frac{\partial^2(K_z C_j)}{\partial z^2} + \Phi \end{aligned} \quad (1)$$

where C_j is the mass concentration of particles (kg m^{-3}) in a given grain-size category j , t is the

time (seconds), x , y and z are components of a rectangular coordinate system (metres), with corresponding velocity components u_x , u_y and u_z (m s^{-1}), and corresponding diffusion-coefficient components K_x , K_y and K_z ($\text{m}^2 \text{s}^{-1}$). Φ is a source or sink term that can be used to describe the change in particle concentration with time ($\text{kg m}^{-3} \text{s}^{-1}$).

Some of the models based on equation (1) describe tephra dispersion as advection of particles from plumes approximated as vertical line diffusers located on the position of the eruptive vent (e.g. Suzuki 1983; Armienti *et al.* 1988; Macedonio *et al.* 1988; Glaze & Self 1991; Hurst & Turner 1999; Bonadonna *et al.* 2005; Pfeiffer *et al.* 2005) and co-pyroclastic-flow sources (Bonadonna *et al.* 2002a). To simplify the algorithm even further, some workers have also modified equation (1) by making some assumptions, such as constant terminal velocity with particle size, constant and isotropic horizontal diffusion coefficient (i.e. $K = K_x = K_y$), negligible vertical diffusion (i.e. $K_z = 0$) and negligible vertical wind velocity (e.g. Armienti *et al.* 1988; Bonadonna *et al.* 2002a). Based on these assumptions, equation (1) can be written as

$$\begin{aligned} \frac{\partial C_j}{\partial t} + w_x \frac{\partial C_j}{\partial x} + w_y \frac{\partial C_j}{\partial y} - v_j \frac{\partial C_j}{\partial z} \\ = K \frac{\partial^2 C_j}{\partial x^2} + K \frac{\partial^2 C_j}{\partial y^2} + \Phi \end{aligned} \quad (2)$$

where w_x and w_y are the x and y components of the wind velocity (m s^{-1}), K is the diffusion coefficient ($\text{m}^2 \text{s}^{-1}$) and v_j is the settling velocity of the particles of the size class j (m s^{-1}). Equation (2) can also be slightly modified to account for the variation of particle terminal velocity with height as a result of the variation of particle Reynolds number and atmospheric density. In this case, v is determined for each size class j and each atmospheric interval k (e.g. Bonadonna *et al.* 1998, 2005; Connor & Connor 2006) (Fig. 2).

The quantity of greatest interest in hazard studies is the mass accumulation, M , at a point (x, y) on the ground, which represents the sum of all particle sizes, j , released from all levels, l (Fig. 2). The mass accumulation is calculated by

$$M(x, y) = \sum_{l=0}^H \sum_{j=d_{\min}}^{d_{\max}} m_{l,j}(x, y) \quad (3)$$

where $m_{l,j}(x, y)$ is the mass fraction of the size class j released from the level l accumulated at (x, y) , H is the total plume height and d_{\min} and d_{\max} are the minimum and maximum particle diameter,

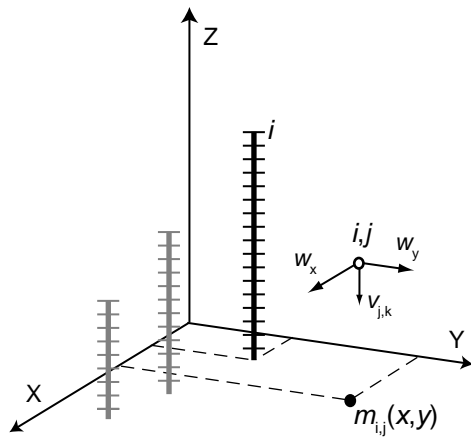


Fig. 2. Simplified sketch showing the rectangular coordinate system. Vertical lines represent the simulated volcanic plumes of coordinates x and y : the black line represents the plume on the main eruptive vent; grey lines represent co-pyroclastic flow plumes overriding pyroclastic flows. Horizontal segments represent particle-releasing points l . Each particle (\circ), corresponding to a size class j , is advected by atmospheric wind described by the two vectors w_x and w_y , and moves downward according to its terminal velocity determined for each atmospheric level k . $m_{i,j}(x, y)$ represents the accumulation of tephra on the ground at a point (x, y) of particles of size j released from a level l (equation (3)).

respectively (Armenti *et al.* 1988; Bonadonna *et al.* 2005; Connor & Connor 2006).

These models are based on the assumption that, far from the source, the eruption-column dynamics is negligible and particle dispersion and sedimentation are mainly controlled by wind transport, turbulent diffusion and settling caused by gravity. In addition, complex plume and atmospheric processes are typically lumped into empirical parameters, such as the term K in equation (2). This greatly simplifies the models but also ignores processes that can affect tephra dispersion, such as the variation of the diffusion coefficient with barometric pressure in the atmosphere and with the scale of the phenomenon. However, given the simplicity of the approach, these models are very versatile and find their ideal application in the computationally expensive simulations required in hazard assessments. Moreover, a thorough investigation of empirical parameters (e.g. K) based on rigorous sensitivity tests and/or inversion techniques (Connor & Connor 2006), typically results in very good agreement between computed and observed accumulation data that well justifies the application to real-case scenarios.

Other models are based on the advection–diffusion equation described above, but also use principles from the classic plume theory and fluid dynamics (Morton *et al.* 1956; Briggs 1969; Turner 1973) to account for more complex current-spreading dynamics and particle sedimentation. As a result, the use of empirical parameters is kept to a minimum but the algorithm is more complicated. Initially, these models could describe symmetrical plumes and particles of uniform density and settling regime (Bursik *et al.* 1992b; Sparks *et al.* 1992), but they have subsequently been developed to account for wind advection of volcanic clouds (Bursik *et al.* 1992a; Koyaguchi & Ohno 2001) and particle transport combined with various processes of particle sedimentation, such as density variation, Reynolds number variation and particle aggregation (Bonadonna & Phillips 2003). However, even though these models give good agreement with field data and laboratory observations, they still mainly describe sedimentation along the dispersal axis and therefore cannot be used to compile 2D maps.

Finally, equation (1) is also used by atmospheric trajectory models that account for global circulation models to investigate the long-range transport of volcanic plumes (Heffter & Stunder 1993; Searcy *et al.* 1998). These models accurately describe the atmospheric processes and simulate the movement of airborne volcanic particles in near real-time following an eruption cloud for the purposes of hazard warning. As a result, these models represent an indispensable tool for hazard mitigation, in particular for aviation purposes, but they do not predict ground deposition. Nevertheless, they could be easily modified to account for sedimentation of tephra, as they have already been used to describe deposition of radioactive and chemical contaminants (Stunder *et al.* 1986; Apsimon *et al.* 1988).

Probabilistic analysis of tephra dispersion

A number of pioneering volcanic hazard assessments have completely relied on characteristics of the stratigraphic record, prevailing geomorphology and some characteristics of the local climate (Crandell & Mullineaux 1978; Wadge & Isaacs 1988). Some researchers have also used a similar approach to that used for earthquakes to quantify the probability of a particular tephra accumulation at any given site based on observations (Stirling & Wilson 2002). As described in the previous two sections, thorough field investigations of tephra deposits provide crucial insights into the history and the characteristics of specific volcanoes. Although extremely important, these studies are not sufficient for a complete understanding of

volcanoes and for the mitigation of their risks. This is certainly true for volcanic environments that are characterized by few past eruptions and for which the resulting deposits are limited or are difficult to interpret. In addition, past eruptions generally provide a limited sample of all possible wind profiles. Finally, given the nature of preservation of pyroclastic deposits, the geological record is typically biased toward larger, less frequent events.

One possible solution to the limitation of field data is probabilistic analysis of a large number of wind profiles and of a large number of activity scenarios and eruptive conditions considered possible. These analyses are often crucial even for volcanoes with a well-known history and relatively frequent eruptions (e.g. Vesuvius, Italy), where field data can be combined with numerical simulations to provide a comprehensive hazard assessment (Cioni *et al.* 2003).

At present, only models from the first category described in the previous section can be realistically used to forecast hazardous tephra accumulation (e.g. Suzuki 1983; Armienti *et al.* 1988). Historically, these advection–diffusion models have been used to investigate the probability distribution of reaching specific hazardous accumulations of tephra given the maximum expected event (Barberi *et al.* 1990; Hill *et al.* 1998). This approach provides more information than the pure deterministic one described above. However, it is still limited by the assumption of the maximum expected event or even the most likely event, which is typically very hard to identify objectively in volcanology (Blong 1996; Marzocchi *et al.* 2004). The formulation of the most likely event or most likely activity scenario is a very delicate issue and several workers have suggested techniques to quantify the probability of volcanic events (Newhall & Hoblitt 2002; Stirling & Wilson 2002; Aspinall *et al.* 2003; Marzocchi *et al.* 2004). Some workers have also used Monte-Carlo simulations to allow uncertainties in the eruption-frequency distributions to be included explicitly when not many field data are available (Hurst & Smith 2004). The evaluation of these procedures is beyond the scope of this paper, but certainly for a comprehensive volcanic hazard assessment, several types of probability analysis should be carried out and different scenarios and volcanic activities should be considered and compared (see the Discussion).

The compilation of any hazard assessment also requires the use of a statistically significant sample of wind profiles. The number of wind profiles used depends on the range of variation characteristic of specific geographical areas; the larger the variation, the larger the number of wind profiles. Selected wind samples can also be used to

investigate specific atmospheric conditions, such as seasonal variations and the El Niño–Southern Oscillation (ENSO) phenomenon (Bonadonna *et al.* 2005). The main types of probability approaches used for hazard mitigation and risk management purposes are described below. Examples from real-case studies are also shown (mainly using data from Bonadonna *et al.* (2002a, 2005)).

Probability maps based on hazardous thresholds

Given an eruptive scenario, these probability maps contour the probability of reaching a particular hazardous accumulation threshold (kg m^{-2}). Hazardous accumulations of tephra can be estimated for specific areas or can be based on the effects of tephra observed for a number of eruptive events and different volcanoes. The most common hazardous thresholds used in hazard assessments are the threshold for minor damage to vegetation, which has significant implications for agriculture (c. $1 \text{ cm} \approx 10 \text{ kg m}^{-2}$, for a deposit density of 1000 kg m^{-3} ; Blong 1984; Bonadonna *et al.* 2002a) and the threshold for the collapse of buildings (c. $100\text{--}700 \text{ kg m}^{-2}$, depending on the structure of the roof). A threshold for airport closure is also important to consider in areas with heavy air traffic (e.g. 1 kg m^{-2}). Other hazardous thresholds are (Blong 1984): 150–500 mm (partial survival of vegetation, zone 2), 500–1500 mm (partial survival of vegetation, zone 1), 1500 mm (zone of near-total vegetation kill) and >1500 mm (zone of total vegetation kill). These four zones are based on vegetation damage around Parícutin during the 1943–1952 eruption: in the zone of total vegetation kill all vegetation died; in the zone of near-total vegetation kill most individuals of all size classes of all species were eliminated; in the first zone of partial survival tree damage and heavy kill of shrubs and herbs occurred; in the second zone of partial survival tephra accumulation resulted in slight tree damage and partial survival of shrubs and herbs.

Individual eruptive episodes.

(1) *Probability maps given one eruptive episode and a set of wind profiles (One Eruption Scenario).* These maps show the probability distribution of reaching a particular tephra accumulation around the volcano based on the statistical distribution of wind profiles and therefore contour $P[M(x, y) \geq \text{threshold} \mid \text{eruption}]$, where all eruption parameters are specified deterministically (e.g. Fig. 3a). $M(x, y)$ is the mass per unit area at a given point with coordinates (x, y) (Fig. 2; equation (3)), and threshold is a given accumulation of tephra considered hazardous (kg m^{-2}). Given a number of

wind profiles N_w , the probability, $P(x, y)$ at a point with coordinates (x, y) is determined by summing the number of times a certain hazardous threshold is reached:

$$P(x, y) = \frac{\sum_{i=1}^{N_w} n_i}{N_w}, \quad (4)$$

where

$$n_i = \begin{cases} 1, & \text{if } [M_i(x, y) \geq \text{threshold|eruption}] \\ 0, & \text{otherwise} \end{cases}$$

where i refers to a given wind profile. The total number of wind profiles N_w is equivalent to the number of runs performed. Any number of wind profiles, N_w , can be used, with each run being independent; that is, the outcome of each run is unaffected by previous runs. One Eruption Scenario maps are useful for determining the upper limit

value on tephra accumulation if the parameters are specified for the largest eruption considered in any given scenario. They are often defined as upper limit scenarios or scenarios for the maximum expected event with the limitation discussed above.

(2) *Probability maps given a set of eruptive episodes and a set of wind profiles (Eruption Range Scenario)*. These maps show the probability distribution of a particular mass loading around the volcano based on the statistical distribution of possible eruptive episodes and wind profiles (e.g. Fig. 3b). These maps contour $P[M(x, y) \geq \text{threshold|eruption}]$, where all eruption parameters and wind profiles are randomly sampled, and provide a fully probabilistic hazard assessment for the investigated activity scenario. The probability $P(x, y)$ at a point with coordinates (x, y) is determined using equation (4), where for each run, i , the eruption parameters are sampled from a given function instead of being specified deterministically.

(3) *Probability maps given a set of eruptive episodes and one wind profile (One Wind Scenario)*. These maps show the probability distribution of a particular mass loading around the volcano based on the statistical distribution of possible eruptive episodes and one wind profile. These maps contour $P[M(x, y) \geq \text{threshold|wind profile}]$, where all eruption parameters are randomly sampled and the wind profile is chosen *a priori*. Given N_e , the total number of possible eruptions considered, the probability, $P(x, y)$, at a point with coordinates (x, y) , is determined by summing the number of times a certain hazardous threshold is reached:

$$P(x, y) = \frac{\sum_{i=1}^{N_e} n_i}{N_e}, \quad (5)$$

where

$$n_i = \begin{cases} 1, & \text{if } [M_i(x, y) \geq \text{threshold|wind profile}] \\ 0, & \text{otherwise} \end{cases}$$

where i refers to a given eruption. These maps are used for hazard assessments of specific sites (e.g. nuclear power plants). In such cases the worst-case scenario is considered with the wind blowing in the direction of the considered site (McBirney & Godoy 2003; McBirney *et al.* 2003).

Long-lasting activity (i.e. total accumulation probability maps). These maps show the probability distribution of reaching a particular mass loading around the volcano given the statistics of winds and a certain activity scenario; that is, many

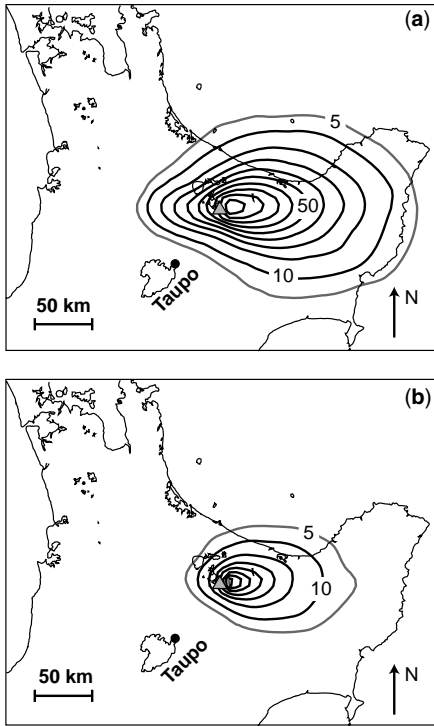


Fig. 3. (a) One Eruption Scenario and (b) Eruption Range Scenario computed for the tephra hazard assessment of Tarawera volcano, New Zealand (see text for the input parameters used). Contour interval is 10% probability of reaching the hazardous threshold of minor damage to vegetation (i.e. 10 kg m^{-2}). The 5% contour is also shown (grey contour). Tarawera volcano (\blacktriangle) and the city of Taupo (\bullet) are also shown.

eruptive episodes with different magnitudes and/or of different types occurring over a certain period of time, contouring $P[M(x, y) \geq \text{threshold}|\text{scenario}]$. These maps are important for assessing tephra accumulation from multi-phase eruptions, for example, the *c.* AD 1315 Kaharoa eruption of Tarawera volcano, New Zealand (Sahetapy-Engel 2002), and long-lasting eruptions, for example, the 1995–present eruption of The Soufrière Hills volcano, Montserrat (Kokelaar 2002). Table 1 shows an example of activity scenario used for the hazard assessment of the Soufrière Hills volcano and based on the 1995–1998 eruptive activity. These maps are more complex than probability maps compiled for individual events, as they need to include individual probabilities of individual eruptive events, and combinations of wind profiles and accumulation or erosion of tephra deposits over a certain period of time. As the process of erosion cannot be easily predicted, maximum and minimum accumulation probabilities can be investigated. The actual tephra accumulation for a specific activity scenario is most likely to be between the forecast of these two end-members (*i.e.* minimum and maximum tephra accumulation). The large difference between probability maps for the minimum and maximum accumulation compiled for the hazard assessment on Montserrat has confirmed the importance of clean-up operations during long-lasting eruptions (Bonadonna *et al.* 2002a).

(1) *Total accumulation probability maps for a given scenario of activity and set of wind profiles (Multiple Eruption Scenario for the maximum accumulation).* These probability maps (Fig. 4a and b) assume continuous tephra accumulation with no erosion between eruptive episodes and are calculated using Monte-Carlo simulations based on a random sampling of specific eruption parameters; for example, wind profile and valley of

dome collapse (*i.e.* the valley in which the pyroclastic flow associated with a dome collapse is going to flow) (Bonadonna *et al.* 2002a). The wind profile is random and does not depend on the eruptive episode. The valley of collapse depends on the direction of preferential dome growth, which is assumed to be random. The Monte-Carlo approach is used because for this kind of map it is impracticable to compute the number of combinations of tephra accumulation produced by individual eruptive episodes and wind profiles (Table 1). The probability $P(x, y)$ is determined by adding the contribution from individual eruptive episodes to tephra accumulation at a point with coordinates (x, y) :

$$P(x, y) = \frac{\sum_{i=1}^{N_s} n_i}{N_s}, \quad (6)$$

where

$$n_i = \begin{cases} 1, & \text{if } [M_{\text{TOT}i}(x, y) \geq \text{threshold}|\text{scenario}] \\ 0, & \text{otherwise} \end{cases}$$

where i refers to a given sequence of eruptive episodes. N_s represents the number of times a given sequence (*i.e.* scenario) is performed using a different combination of wind profiles. Wind profiles are randomly sampled for each eruptive episode in each sequence. $M_{\text{TOT}i}(x, y)$ represents the accumulation of tephra produced from all eruptive episodes considered in a given sequence, i . Sequences can consist of either the same eruptive episodes (the most likely scenario) or different eruptive episodes (a range of possible scenarios).

Examples of these maps were used for the hazard assessment of Tarawera (*i.e.* multi-phase eruption; Bonadonna *et al.* 2005) and Soufrière Hills (long-lasting eruption, Fig. 4a–b); Bonadonna *et al.* 2002a). The Multiple Eruption Scenario assessment of Soufrière Hills was based on the most likely scenario, whereas the Tarawera assessment was based on a range of possible scenarios. In fact, for the Montserrat assessment, only the sequence in Table 1 was performed in association with different combinations of wind profiles and valleys of collapse, whereas for the Tarawera assessment each sequence i consisted of 10 Plinian eruptions randomly sampled. The Tarawera assessment was based on the *c.* AD 1315 Kaharoa eruption sequence, which consisted of 10 Plinian eruptive episodes with plume height ranging between 14 and 26 km above sea level. However, field data for this eruption sequence are limited and did not allow for the most likely scenario of activity to be easily constrained (Bonadonna *et al.* 2005). As a result, plume heights, eruption

Table 1. Activity scenario used for the hazard assessment of tephra dispersion on Montserrat (approximation of the July 1995–March 1998 activity)

Event	Volume, DRE ($\times 10^6 \text{ m}^3$)	Number of events (3 year period)
Dome collapse	50	1
Dome collapse	30	1
Dome collapse	10	2
Dome collapse	3	7
Dome collapse	1	16
Dome collapse	0.5	30
Vulcanian explosions	0.4	90

Volume is given as dense rock equivalent (DRE), an estimate of the volume of erupted unvesiculated magma.

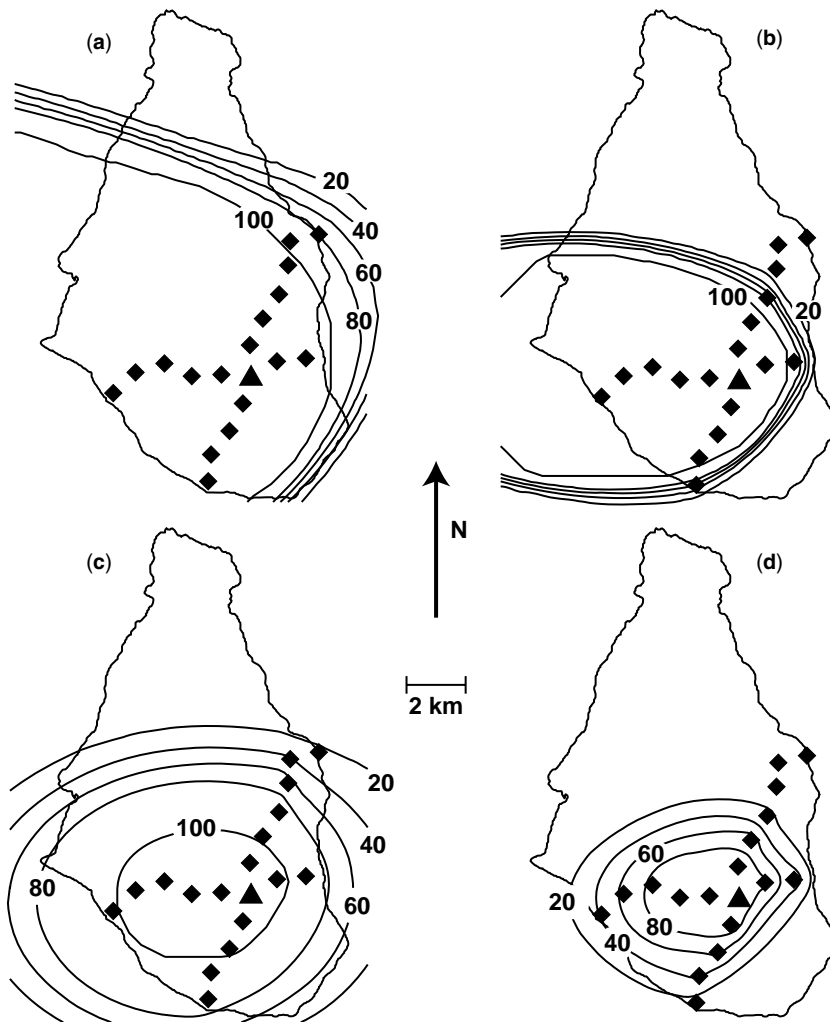


Fig. 4. Multiple Eruption Scenario (MES) maps computed for the activity scenario in Table 1. MES for the maximum tephra accumulation and a threshold of (a) 12kg m^{-2} and (b) 120kg m^{-2} . MES for the minimum tephra accumulation and a threshold of (c) 12kg m^{-2} and (d) 120kg m^{-2} . These thresholds are for minor damage to vegetation and minimum accumulation causing roof collapse adapted for a deposit density of 1200kg m^{-3} . The computed coproclastic-flow plume sources (\blacklozenge) and the Soufrière Hills volcano (\blacktriangle) are also shown. Contour interval is 20% probability. Maps were computed using 3 years of wind profiles (1995–1997). MES maps for the maximum accumulation are based on 200 Monte-Carlo simulations.

durations, total grain-size distributions and eruptive vents were randomly sampled from specific probability density distributions (see the next section for details).

For the Montserrat study, the accuracy of the Monte-Carlo simulations was investigated by calculating several times the probability of reaching a certain deposit threshold (12kg m^{-2}) at a particular locality for different numbers of runs and for different samples of wind profiles (1, 3 and 6 years)

(Fig. 5a). The standard deviation for the three wind samples decreases with the number of runs, but does not vary significantly with the number of wind profiles used (Fig. 5b). The variation of this standard deviation is fitted well by a power law (Fig. 5b). The mean probability also does not vary significantly for the three samples of wind profiles used (Fig. 5c) (standard deviation of the mean probability of the three samples of wind profiles is 0.7, 0.6 and 0.8 for 1 year, 3 years and 6 years,

respectively). In conclusion, for this particular geographical and volcanic setting, probability maps are much more sensitive to the number of Monte-Carlo simulations considered than to the number of wind profiles sampled.

(2) *Total accumulation probability maps for a given scenario of activity and a set of wind profiles (Multiple Eruption Scenario for the minimum accumulation).* These maps differ from maximum

accumulation maps because they assume erosion between events. In this case the probability of reaching a specific hazardous threshold is calculated separately for each eruptive episode considered in the scenario (Fig. 4c and d; Table 1), and then the total accumulation probabilities are calculated by the union of individual probabilities of each episode. Over a certain period of activity, different eruptive episodes represent independent, but not mutually exclusive, events. To fully understand this concept, let us consider some basic principles of probability theory. When an experiment is performed whose outcome is uncertain, the collection of possible elementary outcomes is called sample space, often denoted by S . For any two events, A_1 and A_2 , of a sample space, S , we define the new event, $A_1 \cup A_2$, to consist of all points that are either in A_1 or in A_2 or in both A_1 and A_2 . That is, the event, $A_1 \cup A_2$ will occur if either A_1 or A_2 occurs. The event, $A_1 \cup A_2$ is called the union of the events A_1 and A_2 (Fig. 6a). For any two events, A_1 and A_2 , we may also define the new event, $A_1 \cap A_2$ (or A_1A_2), called the intersection of A_1 and A_2 , to consist of all outcomes that are both in A_1 and in A_2 . That is, the event, A_1A_2 , will occur only if both A_1 and A_2 occur (Fig. 6b). If $A_1A_2 = \emptyset$, then A_1 and A_2 are said to be mutually exclusive (where \emptyset is the empty set relative to S). Finally, for any event, A_1 , we define the new event, A_1^C , referred to as the complement of A_1 , to consist of all points in the sample space, S , that are not in A_1 (Fig. 6c). That is, A_1^C will occur if and only if A_1 does not occur. A_1 and A_1^C are always mutually exclusive.

Eruptive episodes of a specific activity scenario are independent but not mutually exclusive because they have no influence on each other and they all happen. Let A_1 and A_2 be the probability $P(x, y)$ determined using equation (4) for the eruptive episodes 1 and 2, respectively. The probability of the union of A_1 and A_2 is

$$P(A_1 \cup A_2) = P(A_1) + P(A_2) - P(A_1 \cap A_2) \quad (7)$$

and, as A_1 and A_2 are independent,

$$P(A_1 \cap A_2) = P(A_1)P(A_2). \quad (8)$$

Resolving equation (7) for n events,

$$\begin{aligned} P(A_1 \cup A_2 \cup \dots \cup A_n) &= \sum_{i=1}^n P(A_i) - \sum_{i_1 < i_2} P(A_{i_1}A_{i_2}) + \dots + \\ &(-1)^{r+1} \sum_{i_1 < i_2 < \dots < i_r} P(A_{i_1}A_{i_2} \dots A_{i_r}) + \dots + \\ &(-1)^{n+1} P(A_1A_2 \dots A_n). \end{aligned} \quad (9)$$

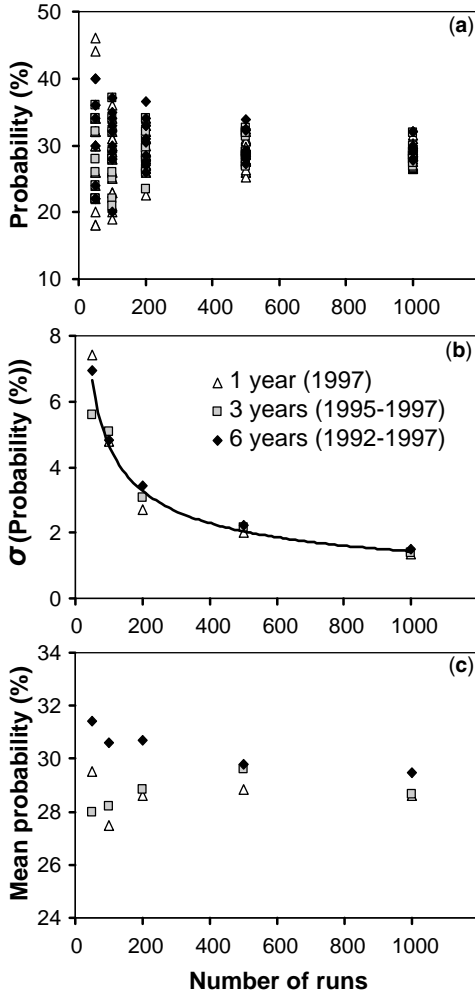


Fig. 5. Accuracy of the Monte-Carlo technique used to compile Multiple Eruption Scenario maps for the maximum tephra accumulation (Fig. 4a). Variability of: (a) probability values; (b) standard deviation of probability values (corresponding power-law fit is also shown); (c) mean of probability values. Probability values were computed for a given locality and a threshold of 12 kg m^{-2} . Simulations for any given number of runs were performed 20 times for the case of 1 year period and 10 times for the cases of 3 and 6 year periods.

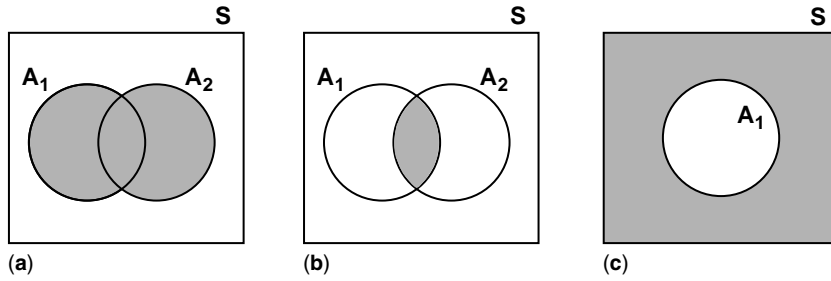


Fig. 6. Venn diagrams showing the subspace S (consisting of all the points in the rectangle) and the events A_1 and A_2 (consisting of all the points in given circles within the rectangle). Shaded areas show events of interest: (a) $A_1 \cup A_2$ (union); (b) $A_1 \cap A_2$ (intersection); (c) A_1^C (complement).

The summation $\sum_{i_1 < i_2 < \dots < i_r} P(A_{i_1} A_{i_2} \dots A_{i_r})$ is taken over all of the $\binom{n}{r}$ possible subsets of size r of the set $\{1, 2, \dots, n\}$ (Ross 1989). An equivalent solution for the same problem is obtained by calculating the probability of the intersection of all the complements $A_1^C, A_2^C, \dots, A_n^C$, to analyse the probability of 'never reaching a certain hazardous threshold at a given grid point given a scenario of activity'. This probability can be described as

$$P(A_1 \cup A_2 \cup \dots \cup A_n) = 1 - P(A_1^C) \times P(A_2^C) \times \dots \times P(A_n^C). \quad (10)$$

An example of these maps was used for the hazard assessment of the Soufrière Hills volcano (Fig. 4c and d).

Hazard curves for tephra accumulation

All the scenarios discussed above can also be used to compile hazard curves, which typically show the probability of exceeding certain values of accumulation of tephra per unit area at a particular location (Hill *et al.* 1998; Stirling & Wilson 2002). Hazard curves are more commonly known in statistics as survivor or complementary cumulative distribution functions, because they plot probability complements v. sorted values of interest (e.g. tephra accumulation in Fig. 7). However, they are very different from hazard functions, which represent the ratio between probability density functions and survivor functions.

For X , the random variable specifying tephra accumulation, what is the exceedance probability $EP = P(X > x)$, where x is a specific mass per unit area? For example, what is the probability that tephra accumulation will exceed $x = 10 \text{ kg m}^{-2}$? Outputs of tephra accumulation from dedicated numerical simulations can be sorted in ascending order, $X_0, X_1, X_2, \dots, X_{N-1}$, then

$$EP_i = 1 - \frac{i}{N}, \quad \text{for } 0 \leq i < N. \quad (11)$$

These curves are limited to a certain locality but are more flexible than probability maps as they do not rely on the choice of hazardous thresholds (e.g. Fig. 7).

Hazard curves can also be constructed from field data at a particular locality by sorting observed tephra accumulations in ascending order and deriving the exceedance probability from equation (11) (e.g. dashed line in Fig. 8). However, the stratigraphic record can be misleading because it does not provide a wide range of accumulation values for individual localities and, mainly because of erosion, it is typically biased towards the largest events. The difference between computed curves (continuous lines) and the curve constructed from field data (dashed line) can be defined as reducible or epistemic uncertainty; that is, uncertainty caused by lack of information (see the Discussion). As a result, geological records are not detailed enough to investigate low-probability events. For instance, the field-based curve stops at probability exceedance *c.* 3% in Fig. 8, whereas the computed curves can be extrapolated down to 0.1%

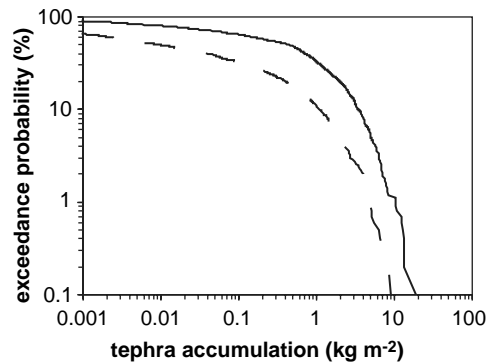


Fig. 7. Hazard curves computed for the One Eruption Scenario (continuous line) and the Eruption Range Scenario (dashed line) for the city of Taupo. Location of Taupo is indicated in Fig. 3.

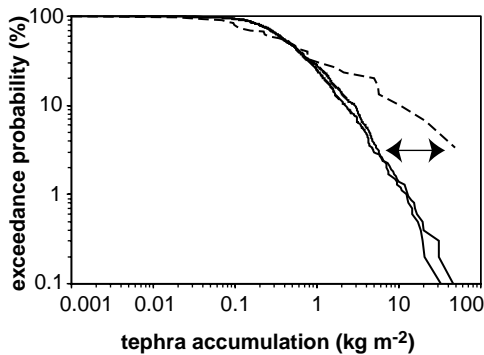


Fig. 8. Comparison between two hazard curves computed using two different random generator functions (continuous lines) and a hazard curve derived from field data (dashed line) for the same locality. Field data were collected on Montserrat between 3 June 1996 and 27 June 1997 at a location about 4 km west of the Soufrière Hills volcano (Bonadonna *et al.* 2002b). Computed curves were generated running 1000 Monte-Carlo simulations and considering a scenario that approximates the 1996–1997 activity of the Soufrière Hills volcano. Such a scenario predicts the occurrence of dome collapses with volume 0.5, 1, 3 and $10 \times 10^6 \text{ m}^3$ with a corresponding probability of 54%, 29%, 13% and 4%, respectively. The difference between the computed and field-based hazard curves depends on the epistemic uncertainty (double-headed arrow).

probability or even lower if more Monte-Carlo runs are performed.

It is important to notice that the Soufrière Hills volcano record is one of the most detailed stratigraphic records available in the volcanology literature (e.g. the field-based curve in Fig. 8 is derived from 30 sample collections at the same locality over a 1 year period). In addition, Soufrière Hills volcano tephra is typically collected during fallout using dedicated containers, and therefore small accumulations can be accounted for. Stratigraphic records from less studied areas are expected to provide even larger epistemic uncertainties.

Finally, stratigraphic records typically represent a very small sample of all possible activity scenarios. For example, the Soufrière Hills volcano geological record between June 1996 and June 1997 (Fig. 8) does not account for the significantly larger dome collapses that occurred in late 1997 ($c. 45 \times 10^6 \text{ m}^3$ dense rock equivalent (DRE), Boxing Day collapse) and in 2003 ($c. 210 \times 10^6 \text{ m}^3$, DRE; 12–15 July 2003 collapses), or the 88 Vulcanian explosions that occurred in August–October 1997. In conclusion, a careful analysis of possible activity scenarios combined with dedicated numerical simulations and probability calculations provides a more reliable hazard assessment than general assessments based only on stratigraphic records.

Probability maps and hazard curves based on return periods

Given an erupted volume frequency distribution for one or more volcanoes, probability maps can be compiled to contour the tephra accumulation with a particular return period (e.g. 10 ka) and hazard curves can be constructed to plot the return period as a function of tephra accumulation (Fig. 9; Hurst & Smith 2004). This approach is particularly valuable for risk management purposes; for example, for insurance companies. In fact, insurance companies are more interested in the probability of reaching a hazardous accumulation of tephra at a given location in a given period of time than in the hazard assessment in terms of eruptive scenario as discussed above. Hazard assessments in terms of eruptive scenario are more

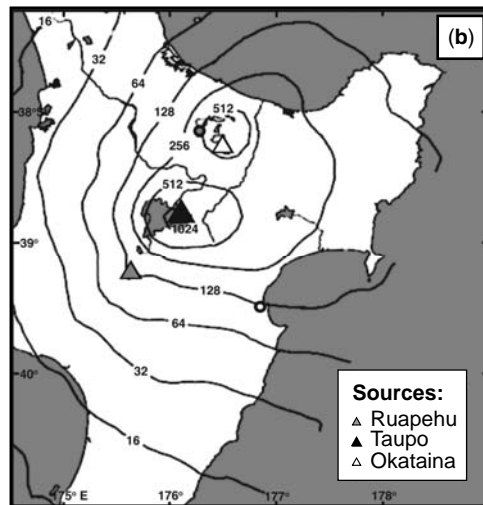
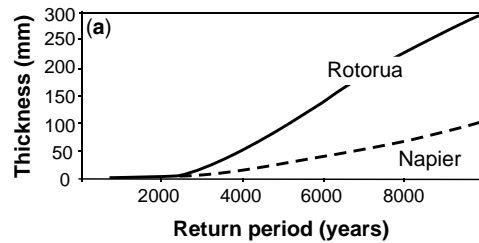


Fig. 9. (a) Return period as a function of tephra thickness (mm) for the combined effects of Ruapehu, Taupo and Okataina eruptions at the cities of Rotorua and Napier, New Zealand. (b) Map of the North Island of New Zealand showing tephra thickness (mm) with a 10 ka return period (i.e. 1/10 000 annual probability) based on eruptions from Ruapehu, Taupo and Okataina. The grey and white circles indicate the cities of Rotorua and Napier, respectively. Data and map from Hurst & Smith (2004).

valuable for planning purposes and hazard mitigation, because an effort is made to present realistic scenarios and likely effects (Hurst & Smith 2004). As a result, the return-period approach relies on a careful quantification of the volcanic eruption history, and therefore is typically more complex than the eruptive-scenario approach because reliable field data on the eruption frequency distributions are rarely available.

Probabilistic analyses of input parameters

A random sampling can be used to identify not only wind profiles but a whole range of input parameters for the physical model (e.g. column height, eruption duration, total grain-size distribution, eruptive vent). This is important because sometimes different eruptive scenarios need to be investigated but also because often these parameters are not well known but can be sampled from probability density functions. Therefore, the more simulations are performed the better the full range of possible outcomes is understood. This kind of Monte-Carlo approach is very similar to the ensemble forecast technique commonly used in weather and climate forecast to deal with the uncertainties of models and/or perturbed initial conditions (Palmer 2000). For instance, the Multiple Eruption Scenario assessment for Tarawera volcano performed running different sequences of eruptive episodes associated with a range of plume heights, total grain-size distributions, eruption durations and eruptive vents can be considered as an example of ensemble forecast for tephra dispersion (Bonadonna *et al.* 2005). Such an assessment provides a comprehensive analysis of possible outcomes in a situation where the stratigraphic record does not allow for detailed scenarios to be constrained. It differs from ensemble forecasts used in meteorology because these mainly combine outputs derived with different models (Palmer 2000). Any probability density function for input parameters can be used. In a case where the history of the volcano is well known, the probability density function can be based on field data (Cioni *et al.* 2003); in a case where not many observations are available, the probability density function can be derived from Monte-Carlo simulations based on the few data available (Hurst & Smith 2004) or arbitrarily chosen based on some general criteria for natural processes (Bonadonna *et al.* 2005). For instance, in the Eruption Range Scenario and the Multiple Eruption Scenario used for the assessment of a multi-phase eruption at Tarawera volcano, the column height was sampled from a uniform set of values ranging between $\log(H_{\min})$ and $\log(H_{\max})$, where H_{\min} and H_{\max} are the minimum and the maximum plume height observed and/or

considered possible (14 km and 26 km in this case). The logarithmic function was chosen to reflect a natural higher frequency of low plumes. In the same assessment, because of limitations of field data, the total grain-size distribution was uniformly sampled amongst three distributions derived for a different New Zealand volcano with similar characteristics. Finally, based on field observations from the Kaharoa eruption, the eruption duration was uniformly sampled between 2 and 6 h and the eruptive vent was uniformly sampled from three locations within the Tarawera volcanic complex (Bonadonna *et al.* 2005).

Discussion

Importance of probability analysis

Field observations of tephra deposits (e.g. Fig. 1), are crucial to our understanding of the history and the behaviour of a volcano. However, hazard assessments of tephra accumulation cannot be based on field observations only, and they also require a thorough probabilistic analysis of a wide range of possible scenarios. In fact, field observations are the result of a few eruptive conditions that are typically not statistically meaningful. For instance, the geological record samples only a few column heights, eruption durations and wind profiles. In particular, wind profiles are typically very variable and field observations are too limited to represent a statistically significant sample of weather conditions. Any sample of wind data used for numerical simulations (e.g. 1, 5 or 10 years, or more) will always be a subsample of the whole possible range, but still more significant than the range shown in the stratigraphic record. A careful analysis of wind profiles can provide an indication of the critical number of wind profiles that needs to be considered to capture the variability significantly relevant in specific hazard studies (e.g. Fig. 5). In addition, the combination of direct observations of tephra accumulation and the study of the resulting deposits has often shown that only the major eruptive episodes leave a significant stratigraphic record, whereas smaller episodes produce tephra deposits that are typically eroded soon after they have been deposited (Bonadonna *et al.* 2002b). Therefore, a hazard assessment based only on the stratigraphic record would be clearly biased toward large events. This is particularly true for prehistoric stratigraphic records, which are more likely to have experienced erosion, especially of thin layers. In short, the stratigraphic record sampled at a given location typically represents an incomplete accumulation curve, whereas a hazard curve compiled for the same location represents a comprehensive forecast that also accounts for the

smallest events, for large events that have not happened yet and for a wider range of wind profiles (e.g. Fig. 8). The reliability of such a forecast is obviously based on the reliability of the activity scenario chosen and the physical model used.

Importance of field data

Field observations are crucial for the calibration of dispersion models and for the identification of possible activity scenarios. First of all, before probability maps and hazard curves are compiled, sensitivity tests need to be carried out to investigate the actual agreement between field and computed data and establish confidence that a given model can actually reproduce the volcanic processes we want to forecast. Second, sensitivity tests based on the comparison between field and computed data are also used to determine empirical parameters that cannot be determined *a priori*. In fact, dispersion models used for hazard assessments still require empirical parameters (e.g. the diffusion coefficient in equation (2)) that mainly account for those complex volcanic processes that these simplified models do not describe, and therefore they need to be determined for each specific volcano and style of eruption. Third, the history of a volcano needs to be carefully studied to produce density functions for the input parameters (e.g. column height, eruption duration, total grain-size distribution, eruptive vent) and to understand the type of activity that characterizes a given volcano. As a result, a hazard assessment is typically very specific for any given volcano and can only be done in combination with field investigations.

Uncertainty analysis

Uncertainty analysis is also an important aspect of numerical studies and probability investigations. Uncertainties can be divided into aleatoric and epistemic. Aleatoric uncertainties are mainly due to random errors in field measurements and to the random behaviour of the natural system. Epistemic uncertainties are due to lack of information of both field data and numerical investigations, and therefore they can represent the inaccuracy of field techniques, the limitation of the geological records and the limitations of the physical model. Often, aleatoric uncertainty can be assessed quantitatively, but realistically epistemic uncertainty may be more important. As a result, probability assessments may be more reliable if they simply give a range of probability values. Epistemic uncertainties can also be reduced by improving our physical models and our field investigation techniques. As a first approximation, numerical simulations typically performed for hazard assessments show good

agreements with field data because uncertainties caused by the physical models (epistemic) are on the same scale as the uncertainties related to the collection of field data (epistemic and aleatoric). As a result, hazard assessments based on these models can be considered reliable. However, physical models still need to be improved to account for parameters that can be crucial for specific eruptive conditions, such as particle aggregation and mass distribution in the convective region of the plume. Propagation of uncertainties in numerical simulations should also be addressed to evaluate the cumulative uncertainties related to the outputs. This represents a complex task, in particular for complex physical models.

Choice of activity scenarios

Hazard assessments discussed in this paper mainly involve conditional probabilities; that is, given a specific eruptive scenario, what is the expected range of tephra accumulation over a region of interest? Once the choice of the eruptive scenario is defined (One Eruption Scenario, Eruption Range Scenario, One Wind Scenario, Multiple Eruption Scenario) and the density functions for input parameters are identified, the assessment becomes relatively straightforward and the various probability techniques described in this paper can be applied. More complicated is the actual choice of the most likely scenario and the maximum expected event (strictly related to the choice of the input parameters). In fact, the maximum expected event often represents the most likely maximum expected event instead of the maximum event possible. Therefore a whole range of events with magnitude or VEI (Volcano Explosivity Index) larger than the most likely maximum expected event is typically ignored, underestimating the actual hazard. As an example, the hazard assessment for the Soufrière Hills volcano was based on the 1996–1998 activity (Table 1; Bonadonna *et al.* 2002a), and it underestimated the upper limit scenario. In fact, the largest dome collapse considered had a volume of $50 \times 10^6 \text{ m}^3$ DRE (Table 1). However, on July 2003 a collapse of $210 \times 10^6 \text{ m}^3$ occurred, causing roof collapses in the SW of the island not predictable by the 1996–1998 scenario. A more comprehensive evaluation of activity scenarios should be based on a critical probability analysis of all possible events (also the most unlikely). As a result, the probability of each scenario could be combined with the probability of reaching a certain tephra accumulation in a given area for a specific scenario. A different approach is the use of ensemble forecast techniques based on random sampling of a wide range of input parameters (including extreme values). In this case, the

density function of input parameters is crucial. For instance, the Multiple Eruption Scenario assessment based on a range of possible scenarios (Tarawera assessment) provides more information and accounts for more possible outcomes than the Multiple Eruption Scenario based on the most likely scenario (Montserrat assessment). The ensemble forecast approach used for Tarawera was made possible by the parallelization of the algorithm. The choice of the eruptive scenario and the maximum expected event will always be biased by the geological record. Therefore, extreme care is required in the investigation of the chosen activity scenario (i.e. chosen input parameters and probability density functions) and researchers need to be aware of the associated limitations and implications for hazard assessments.

Computing implications

Hazard investigations can be computationally expensive because the same calculations need to be executed for a large number of grid points (hazard-map resolution) and several simulations need to be run to analyse a wide range of possible scenarios (hazard-map reliability). The hazard-map reliability also depends on the physical model and on the initial assumptions considered, and these are often simplified to speed up the calculations (e.g. assumption of constant particle settling velocity (Armienti *et al.* 1988; Macedonio *et al.* 1988; Barberi *et al.* 1990; Bonadonna *et al.* 2002a); assumption of uniform wind field (Connor *et al.* 2001); assumption of a single particle diffusion law (Armienti *et al.* 1988; Macedonio *et al.* 1988; Barberi *et al.* 1990; Connor *et al.* 2001; Bonadonna *et al.* 2002a)). One low-cost solution for the improvement of hazard-map resolution, hazard-map reliability and computing time is the use of parallel modelling. Modelling for hazard assessments is embarrassingly parallel because the same calculations are performed independently on a large number of grid points. In this case, computational time is significantly reduced by dividing the number of grid points between several computers (or nodes) and computational speed increases linearly with the number of computers (or nodes) used. As a result, the parallelization of the algorithm increases the computing speed and, therefore, allows for the implementation of the physical model, a fully probabilistic analysis of inputs and outputs (including ensemble-forecast approaches), and the use of denser and larger grids.

Concluding remarks

Hazard assessments of volcanological hazards have significantly progressed during the last 20 years in

association with the development of more powerful computing techniques. Researchers have realized that deterministic assessments typically give limited results that could often be misleading because of the natural bias of geological records. Accounting for a more comprehensive range of possible scenarios, the combination of field data, numerical modelling and probabilistic analysis gives a better understanding of natural processes and their effects. However, such a combination is not always straightforward and requires a critical evaluation of crucial steps.

Reliable field data represent the cornerstone of any hazard study, but for comprehensive hazard assessments, their collection and processing should adjust to the requirements of numerical modelling and probability analyses. In particular, distribution of tephra accumulation should be quantified using isomass maps, complete grain-size distribution for the whole deposit should be determined, the contour line of approximately zero mass should be identified, deposit and particle density should be characterized, and stratigraphic records should be carefully described to define accurate eruptive scenarios. For a comprehensive validation of numerical models, particular attention should be paid to field data from large eruptions. In fact, most good datasets available in the literature to date are from more frequent, weak eruptions, which are typically characterized by very different plume and sedimentation dynamics.

Before considering field observations for validation purposes or to construct specific scenarios, researchers need to fully understand the implications of data-gathering processes and critically evaluate the uncertainties related to individual datasets and the field techniques used. In addition, whenever probabilistic methods are used, uncertainties in the analysis also need to be addressed. Misconception on the capability and limitations of probabilistic approaches and misinterpretations of field data can lead to misleading hazard assessments.

The reliability of hazard assessments is also based on the reliability of the physical model. Current physical models typically used for hazard studies provide good agreement with field data when thorough calibrations are performed. However, recent advances in parallel computing and faster computers allow more complexities in the algorithm, which could help reduce the number of empirical parameters, making the physical models more flexible and easier to use. Therefore, future research should aim toward more robust physical models that can describe also complex but crucial plume and sedimentation processes. For instance, a good parameterization of particle aggregation is necessary to model

dispersion of fine-rich tephra, and a better description of mass distribution in the convective column is required to model tephra dispersion in proximal areas. It would also be important to investigate the evolution of mass distribution with time, the effects of particle shape on terminal velocity, turbulent diffusion and the interaction of the plume with the surrounding atmospheric environment.

Advances in dataset quality and computing techniques, combined with an increasing appreciation for interdisciplinary collaborations, represent a very promising indication for a rapid development of hazard investigations. Resulting studies will provide a fundamental tool for the improvement of life of people living close to active volcanoes.

Further reading

A more extensive review of general characteristics of tephra deposits and numerical modelling of tephra dispersion is given in the book *Volcanic Plumes* by Sparks *et al.* (1997). A detailed description of standard techniques for field investigations and data processing is given in *Volcanic Successions* by Cas & Wright (1987). For a general use of deposit characteristics to determine crucial eruption parameters, the reader is referred to the book *From Magma to Tephra* by Freundt & Rosi (2001).

The author is particularly grateful to S. Sparks, G. Macedonio and C. Connor for their invaluable support and extensive discussions on the application of numerical modelling and probabilistic analysis to hazard assessment of tephra dispersion. She also benefited from constructive considerations on probability investigations from W. Aspinall and W. Marzocchi. Many thanks go to H. Mader, C. Connor and L. Connor for endless encouragement and helpful revisions of this paper.

References

- APSIMON, H. M., GUDIKSEN, P., KHITROV, L., RODHE, H. & YOSHIKURA, T. 1988. Modeling of the dispersal and deposition of radionuclides; lessons from Chernobyl. *Environment*, **30**, 17–20.
- ARMIENTI, P., MACEDONIO, G. & PARESCHI, M. T. 1988. A numerical model for simulation of tephra transport and deposition—applications to May 18, 1980, Mount St Helens eruption. *Journal of Geophysical Research*, **93**, 6463–6476.
- ASPINALL, W. P., WOO, G., VOIGHT, B. & BAXTER, P. J. 2003. Evidence-based volcanology: application to eruption crises. *Journal of Volcanology and Geothermal Research*, **128**, 273–285.
- BARBERI, F., MACEDONIO, G., PARESCHI, M. T. & SANTACROCE, R. 1990. Mapping the tephra fallout risk: an example from Vesuvius, Italy. *Nature*, **344**, 142–144.
- BAXTER, P. J. 1990. Medical effects of volcanic eruptions. 1. Main causes of death and injury. *Bulletin of Volcanology*, **52**, 532–544.
- BLONG, R. J. 1984. *Volcanic Hazards. A Sourcebook on the Effects of Eruptions*. Academic Press, Sydney.
- BLONG, R. J. 1996. Volcanic hazard risk assessment. In: SCARPA, R. & TILLING, R. I. (eds) *Monitoring and Mitigation of Volcanic Hazards*. Springer, Berlin, 675–698.
- BONADONNA, C. & HOUGHTON, B. F. 2005. Total grainsize distribution and volume of tephra-fall deposits. *Bulletin of Volcanology*, **67**, 441–456.
- BONADONNA, C. & PHILLIPS, J. C. 2003. Sedimentation from strong volcanic plumes. *Journal of Geophysical Research*, **108**, 2340–2368.
- BONADONNA, C., ERNST, G. G. J. & SPARKS, R. S. J. 1998. Thickness variations and volume estimates of tephra fall deposits: the importance of particle Reynolds number. *Journal of Volcanology and Geothermal Research*, **81**, 173–187.
- BONADONNA, C., MACEDONIO, G. & SPARKS, R. S. J. 2002a. Numerical modelling of tephra fallout associated with dome collapses and Vulcanian explosions: application to hazard assessment on Montserrat. In: DRUITT, T. H. & KOKELAAR, B. P. (eds) *The Eruption of Soufrière Hills Volcano, Montserrat, from 1995 to 1999*. Geological Society, London, Memoirs, **21**, 517–537.
- BONADONNA, C., MAYBERRY, G. C., CALDER, E. S. *et al.* 2002b. Tephra fallout in the eruption of Soufrière Hills Volcano, Montserrat. In: DRUITT, T. H. & KOKELAAR, B. P. (eds) *The eruption of Soufrière Hills Volcano, Montserrat, from 1995 to 1999*. Geological Society, London, Memoirs, **21**, 483–516.
- BONADONNA, C., CONNOR, C. B., HOUGHTON, B. F., CONNOR, L., BYRNE, M., LAING, A. & HINCKS, T. 2005. Probabilistic modeling of tephra dispersion: hazard assessment of a multi-phase eruption at Tarawera, New Zealand. *Journal of Geophysical Research*, **110**, B03203, doi: 10.1029/2003JB002896.
- BRIGGS, G. A. 1969. *Plume Rise*. US Atomic Energy Commission, Washington, DC.
- BURSIK, M. I., CAREY, S. N. & SPARKS, R. S. J. 1992a. A gravity current model for the May 18, 1980 Mount St Helens plume. *Geophysical Research Letters*, **19**, 1663–1666.
- BURSIK, M. I., SPARKS, R. S. J., GILBERT, J. S. & CAREY, S. N. 1992b. Sedimentation of tephra by volcanic plumes: I. Theory and its comparison with a study of the Fogo A plinian deposit, São Miguel (Azores). *Bulletin of Volcanology*, **54**, 329–344.
- CANUTI, P., CASAGLI, N., CATANI, F. & FALORNI, G. 2002. Modeling of the Guagua Pichincha volcano (Ecuador) lahars. *Physics and Chemistry of the Earth*, **27**, 1587–1599.
- CAREY, S. N. & SIGURDSSON, H. 1982. Influence of particle aggregation on deposition of distal tephra from the May 18, 1980, eruption of Mount St Helens volcano. *Journal of Geophysical Research*, **87**, 7061–7072.

- CAREY, S. N. & SPARKS, R. S. J. 1986. Quantitative models of the fallout and dispersal of tephra from volcanic eruption columns. *Bulletin of Volcanology*, **48**, 109–125.
- CAS, R. & WRIGHT, J. 1987. *Volcanic Successions: Modern and Ancient: a Geological Approach to Processes, Products and Successions*. Springer, Berlin.
- CIONI, R., LONGO, A., MACEDONIO, G., SANTACROCE, R., SBRANA, A., SULPIZIO, R. & ANDRONICO, D. 2003. Assessing pyroclastic fall hazard through field data and numerical simulations: example from Vesuvius. *Journal of Geophysical Research*, **108** (B2), 2063, doi: 10.1029/2001JB000642.
- CONNOR, L. J. & CONNOR, C. B. 2006. Inversion is the key to dispersion: understanding eruption dynamics by inverting tephra fallout. In: MADER, H. M., CONNOR, C. B., COLES, S. G. & CONNOR, L. J. (eds) *Statistics in Volcanology*. Special Publications of IAVCEI, **1**. Geological Society, London, 231–242.
- CONNOR, C. B., HILL, B. E., WINFREY, B., FRANKLIN, N. M. & LA FEMINA, P. C. 2001. Estimation of volcanic hazards from tephra fallout. *Natural Hazards Review*, **2**, 33–42.
- CRANDELL, D. R. & MULLINEAUX, D. R. 1978. Potential hazards from future eruptions of Mt St Helens volcano. *US Geological Survey Bulletin*, **1383C**, 1–26.
- FREUNDT, A. & ROSI, M. 2001. *From Magma to Tephra*. Developments in Volcanology **4**.
- GLAZE, L. S. & SELF, S. 1991. Ashfall dispersal for the 16 September 1986, eruption of Lascar, Chile, calculated by a turbulent-diffusion model. *Geophysical Research Letters*, **18**, 1237–1240.
- HEFFTER, J. L. & STUNDER, B. J. B. 1993. Volcanic Ash Forecast Transport and Dispersion (Vaftad) Model. *Weather and Forecasting*, **8**, 533–541.
- HILL, B. E., CONNOR, C. B., JARZEMBA, M. S., LA FEMINA, P. C., NAVARRO, M. & STRAUCH, W. 1998. 1995 eruptions of Cerro Negro volcano, Nicaragua, and risk assessment for future eruptions. *Geological Society of America Bulletin*, **110**, 1231–1241.
- HURST, A. W. & TURNER, R. 1999. Performance of the program ASHFALL for forecasting ashfall during the 1995 and 1996 eruptions of Ruapehu volcano. *New Zealand Journal of Geology and Geophysics*, **42**, 615–622.
- HURST, T. & SMITH, W. 2004. A Monte Carlo methodology for modelling ashfall hazards. *Journal of Volcanology and Geothermal Research*, **138**, 393–403.
- INMAN, D. L. 1952. Measures for describing the size distribution of sediments. *Journal of Sedimentary Petrology*, **22**, 125–145.
- IVERSON, R. M., SCHILLING, S. P. & VALLANCE, J. W. 1998. Objective delineation of lahar-inundation hazard zones. *Geological Society of America Bulletin*, **110**, 972–984.
- KOKELAAR, B. P. 2002. Setting, chronology and consequences of the eruption of Soufrière Hills Volcano, Montserrat (1995–1999). In: DRUITT, T. H. & KOKELAAR, B. P. (eds) *The Eruption of Soufrière Hills Volcano, Montserrat, from 1995 to 1999*. Geological Society, London, Memoirs, **21**, 1–43.
- KOYAGUCHI, T. & OHNO, M. 2001. Reconstruction of eruption column dynamics on the basis of grain size of tephra fall deposits. 1. Methods. *Journal of Geophysical Research*, **106**, 6499–6512.
- MACEDONIO, G., PARESCHI, M. T. & SANTACROCE, R. 1988. A numerical simulation of the Plinian fall phase of 79 AD eruption of Vesuvius. *Journal of Geophysical Research, Solid Earth and Planets*, **93**, 14817–14827.
- MARZOCCHI, W., SANDRI, L., GASPARINI, P., NEWHALL, C. G. & BOSCHI, E. 2004. Quantifying probabilities of volcanic events: the example of volcanic hazard at Mount Vesuvius. *Journal of Geophysical Research*, **109**, B11201, doi: 10.1029/2004JB003155.
- MCBIRNEY, A. & GODOY, A. 2003. Notes on the IAEA guidelines for assessing volcanic hazards at nuclear facilities. *Journal of Volcanology and Geothermal Research*, **126**, 1–9.
- MCBIRNEY, A. R., SERVA, L., GUERRA, M. & CONNOR, C. B. 2003. Volcanic and seismic hazards at a proposed nuclear power site in central Java. *Journal of Volcanology and Geothermal Research*, **126**, 11–30.
- MORTON, B., TAYLOR, G. L. & TURNER, J. S. 1956. Turbulent gravitational convection from maintained and instantaneous source. *Proceedings of the Royal Society of London*, **234**, 1–23.
- NEWHALL, C. G. & HOBLITT, R. P. 2002. Constructing event trees for volcanic crises. *Bulletin of Volcanology*, **64**, 3–20.
- PALMER, T. N. 2000. Predicting uncertainty in forecasts of weather and climate. *Reports on Progress in Physics*, **63**, 71–116.
- PFEIFFER, T., COSTA, A. & MACEDONIO, G. 2005. A model for the numerical simulation of tephra fall deposits. *Journal of Volcanology and Geothermal Research*, **140**, 273–294.
- PYLE, D. M. 1989. The thickness, volume and grain-size of tephra fall deposits. *Bulletin of Volcanology*, **51**, 1–15.
- ROBERTSON, R., COLE, P., SPARKS, R. S. J., *ET AL.* 1998. The explosive eruption of Soufrière Hills Volcano, Montserrat, West Indies, 17 September, 1996. *Geophysical Research Letters*, **25**, 3429–3432.
- ROSS, S. M. 1989. *A First Course in Probability*. Macmillan, New York.
- SAHETAPY-ENGEL, S. 2002. Tephra fall deposit of the AD 1305 eruption of Tarawera, New Zealand: reconstruction of eruption dynamics. MS thesis, University of Hawaii.
- SEARCY, C., DEAN, K. & STRINGER, W. 1998. PUFF: a high-resolution volcanic ash tracking model. *Journal of Volcanology and Geothermal Research*, **80**, 1–16.
- SPARKS, R. S. J., WILSON, L. & SIGURDSSON, H. 1981. The pyroclastic deposits of the 1875 eruption of

- Askja, Iceland. *Philosophical Transactions of the Royal Society of London*, **229**, 241–273.
- SPARKS, R. S. J., BURSIK, M. I., ABLAY, G. J., THOMAS, R. M. E. & CAREY, S. N. 1992. Sedimentation of tephra by volcanic plumes. 2. Controls on thickness and grain-size variations of tephra fall deposits. *Bulletin of Volcanology*, **54**, 685–695.
- SPARKS, R. S. J., BURSIK, M. I., CAREY, S. N., GILBERT, J. S., GLAZE, L. S., SIGURDSSON, H. & WOODS, A. W. 1997. *Volcanic Plumes*. Wiley, Chichester.
- STIRLING, M. W. & WILSON, C. J. N. 2002. Development of a volcanic hazard model for New Zealand: first approaches from the methods of probabilistic seismic hazard analysis. *Bulletin of the New Zealand Society for Earthquake Engineering*, **35**, 266–277.
- STUNDER, B. J. B., HEFFTER, J. L. & DAYAN, U. 1986. Trajectory analysis of wet deposition at Whiteface Mountain: a sensitivity study. *Atmospheric Environment*, **20**, 1691–1695.
- SUZUKI, T. 1983. A theoretical model for dispersion of tephra. In: SHIMOZURU, D. & YOKOYAMA, I. (eds) *Arc Volcanism, Physics and Tectonics*. Terra, Tokyo, 95–113.
- THORARINSSON, S. 1944. Petrokronologiska Studier på Island. *Geographes Annuales Stockholm*, **26**, 1–217.
- TURNER, J. S. 1973. *Buoyancy Effects in Fluids*. Cambridge University Press, Cambridge.
- WADGE, G. & ISAACS, M. C. 1988. Mapping the volcanic hazards from Soufrière Hills Volcano, Montserrat, West Indies, using an image-processor. *Journal of the Geological Society, London*, **145**, 541–552.
- WADGE, G., YOUNG, P. A. V. & MCKENDRICK, I. J. 1994. Mapping lava flow hazards using computer simulation. *Journal of Geophysical Research-Solid Earth*, **99**, 489–504.
- WADGE, G., JACKSON, P., BOWER, S. M., WOODS, A. W. & CALDER, E. 1998. Computer simulations of pyroclastic flows from dome collapse. *Geophysical Research Letters*, **25**, 3677–3680.
- WALKER, G. P. L. 1971. Grainsize characteristics of pyroclastic deposits. *Journal of Geology*, **79**, 696–714.
- WALKER, G. P. L. 1973. Explosive volcanic eruptions—a new classification scheme. *Geologische Rundschau*, **62**, 431–446.
- WALKER, G. P. L. 1980. The Taupo Pumice: product of the most powerful known (Ultraplinian) eruption? *Journal of Volcanology and Geothermal Research*, **8**, 69–94.

